



Lanthanide Phosphors

Controllable Synthesis, Polymorphism and Structure-Dependent Photoluminescence Properties of Europium Oxyfluorides

HPSTAR
470-2017Ting Wen,^{*,[a,b]} Yannan Zhou,^[a,b] Baocheng Yang,^{*,[a,b]} and Yonggang Wang^{*,[c]}

Abstract: Functional materials that show polymorphism are essential for comparative studies of fundamental structure–property relationships. As a pre-requisite, the establishment of phase-controllable synthetic strategies are especially significant, but still a great challenge at present. We report herein a controllable fluorination route to europium oxyfluorides having various crystal structures, namely, orthorhombic (O), monoclinic (M) and rhombohedral (R) EuOF. This facile fluorination method starts from commercial europium oxide, utilizing poly(tetrafluoroethylene) as the fluorinating agent, and the phase selectivity could be easily achieved by varying the fluorination temperature and Eu/F ratios. The phase evolution and crystal structures of O-, M- and R-EuOF were characterized by ex situ pow-

der X-ray diffraction at different temperatures and Eu/F ratios. Thus, in this way, the crystalline structures of O- and M-EuOF were established for the first time by Rietveld refinement. The steady-state and transient photoluminescence properties of O-, M- and R-EuOF were also studied comparatively and related to their structural features. Despite their similar components, the three EuOF phases exhibit distinct excitation and emission profiles due to subtle divergences in their local structures. Exceptional transition lines were observed for M-EuOF that correspond to energy-transfer processes favoured by its local structural features. These results suggest future lines of investigations of structure–property relationships of functional materials and the rational design of better lanthanide phosphors.

Introduction

Lanthanide oxyfluorides combine the merits of both their fluoride and oxide counterparts, such as low phonon energy, excellent mechanical strength and good chemical and thermal stability. In addition to providing appropriate doping sites for active rare-earth ions (RE³⁺), lanthanide oxyfluorides have proven to be excellent host materials for UV-excited emission (Stokes) or up-conversion (anti-Stokes) generation.^[1] Lanthanide oxyfluorides are also marked by their prevalent polymorphism, such as the cubic fluorite structure, the tetragonal PbFCl-type structure, the rhombohedral SmSI-type structure and the orthorhombic morphology with the so-called Vernier-type incommensurate structure.^[2] The formation of these structures depends on the stoichiometric ratio and the order/disorder arrangement of O²⁻/F⁻ ions in the lattice.^[3] Accordingly, it is possible for a given lanthanide oxyfluoride to crystallize in two or more different structures through specific synthetic routes.

These structure-selective systems are ideal candidates for comparative studies of the structure–property relationships of photoluminescent materials.^[4] For instance, tetragonal and rhombohedral Eu³⁺-doped lanthanum oxyfluorides were crystallized through the Pechini (sol–gel) method at different sintering temperatures and, according to the comparative studies of their fluorescence properties, the different symmetries of the Eu³⁺ sites decided the position of their photoluminescence (PL) divergence.^[5]

Lanthanide ions are characterized by diverse f-orbital configurations that can emit sharp 4f–4f fluorescent outputs or broader 4f–5d emissions. Because f–f transitions are symmetry-forbidden (Laporte rule), the emission behaviour of lanthanide phosphors relies heavily on the local structure of the doping sites. Specifically, Eu³⁺ has been frequently adopted as a structural probe due to its relatively simple energy-level structure and non-degenerate ⁵D₀→⁷F₀ and environment-hypersensitive ⁵D₀→⁷F₂ transitions.^[6] The excitation and emission spectra of Eu³⁺ ions are strongly dependent on the site symmetry of the host lattice, which make them an efficient tool for differentiating subtle coordination environments around the substituted cations.^[7] As a recent example, by investigating the high-resolution PL spectra of Eu³⁺, the breakdown of crystallographic site symmetry in lanthanide-doped α- and β-NaYF₄ (α-NaYF₄: O_h→C_s; β-NaYF₄: C_{3h}→C_s) was successfully revealed.^[8] With respect to lanthanide oxyfluorides, a contrastive Eu³⁺ PL spectral analysis was conducted between Eu³⁺-doped Vernier-phase orthorhombic Y₆O₅F₈ and stoichiometric rhombohedral YOF, which revealed a larger local crystal field anisotropy for YOF.^[9] Evidently, Eu³⁺ ions are an intriguing tool for monitoring the

[a] Institute of Nanostructured Functional Materials, Huanghe Science and Technology College, Zhengzhou, Henan 450006, China
E-mail: tingwen@infm.hhstu.edu.cn
baochengyang@infm.hhstu.edu.cn

[b] Henan Provincial Key Laboratory of Nano-composite materials and Applications, Zhengzhou, Henan 450006, China

[c] Center for High Pressure Science and Technology Advanced Research (HPSTAR), Beijing 100094, China
E-mail: yonggang.wang@hpstar.ac.cn

Supporting information for this article is available on the WWW under <https://doi.org/10.1002/ejic.201700905>.

polymorphic relationships of lanthanide oxyfluorides incorporating the same components.

In our previous work, we synthesized a series of lanthanide oxyfluorides as upconversion (UC) hosts for RE³⁺ doping by a facile fluorination route using poly(tetrafluoroethylene) (PTFE) as the fluorinating agent.^[10] In particular, in the case of erbium oxyfluorides, two crystal morphologies with orthorhombic (O) and rhombohedral (R) structures were achieved, which enabled a comparative study of their phase-dependent UC PL properties.^[11] Owing to the distinct structural features of O- and R-ErOF on the sub-lattice scale, distinct UC PL properties were observed in the two morphologies. Subsequent experiments showed that this PTFE fluorination route could lead to the selective formation of multi-phases of several other RE elements, such as La, Eu, Gd and Lu. Thus, in this work we performed controllable syntheses of europium oxyfluorides with orthorhombic (O), monoclinic (M) and rhombohedral (R) structures by the PTFE fluorination method. The phase-formation conditions of europium oxyfluoride were explored by ex situ powder X-ray diffraction analysis at different reaction temperatures and low-temperature PL spectroscopy was employed to investigate comparatively the local structure and site symmetry of all three phases. The results of these investigations as well as of PL decay measurements are described herein along with a discussion of the mechanism of PL generation in O-, M- and R-EuOF.

Results and Discussion

Phase-Selective Synthesis

We have demonstrated that monoclinic scandium oxyfluoride, orthorhombic Vernier-phase YbOF and orthorhombic and rhombohedral ErOF could be synthesized by the fluorination route adopting PTFE as the fluorinating agent. In the case of europium, we fabricated three phases of EuOF, that is, O-, M- and R-EuOF, achieving phase selectivity by controlling the fluorination temperature and reactant ratio in partially sealed alumina crucibles. Figure 1 shows the PXRD patterns of the products obtained with a fixed Eu₂O₃/PTFE ratio (Eu/F = 1:2) and reaction period (5 h), but at different fluorination temperatures varying from 400 to 1000 °C. Pure O-EuOF was obtained at 500 °C. In the temperature range of 600–800 °C, the diffraction peaks could also be mainly assigned to O-EuOF with small amounts of M-EuOF detected with a similar M/O-EuOF ratio. At 900 °C, both phases (O-EuOF and M-EuOF) disappeared simultaneously, and pure R-EuOF appeared as a phase-pure product; pure R-EuOF was also observed at 1000 °C. Detailed PXRD patterns in the range of 25–35° showing the phase evolution of the O-, M- and R-EuOF polymorphs are provided in Figure S1 in the Supporting Information. As mentioned above, M-EuOF was detected in the temperature range of 600–800 °C, and the diffraction intensity ratios of M-EuOF to O-EuOF were almost the same. We thus considered that the amount of PTFE may influence the formation of M-EuOF in addition to the sintering temperature. Thus, samples were prepared with different mol ratios of Eu/F, namely 1:1.5, 1:2 and 1:2.5, at 600 °C. The PXRD patterns of the products are shown in Figure 2 with

more detailed diffractograms in the range 25–35° shown in Figure S2. For the Eu/F ratio of 1:1.5, the PXRD pattern indicates a mixture of O- and R-EuOF with O-EuOF definitely being the main phase. For the Eu/F ratio of 1:2, O-EuOF and a small amount of M-EuOF were formed, as mentioned above. Finally, M-EuOF was obtained at the Eu/F ratio of 1:2.5 with a small quantity of EuF₃ (ca. 10 % by weight). Despite our great efforts, we found that it was not easy to avoid the formation of a small amount of EuF₃. The PXRD patterns of all three phases, O-, R- and M-EuOF, are compared in the range of 25–35° in Figure 3,

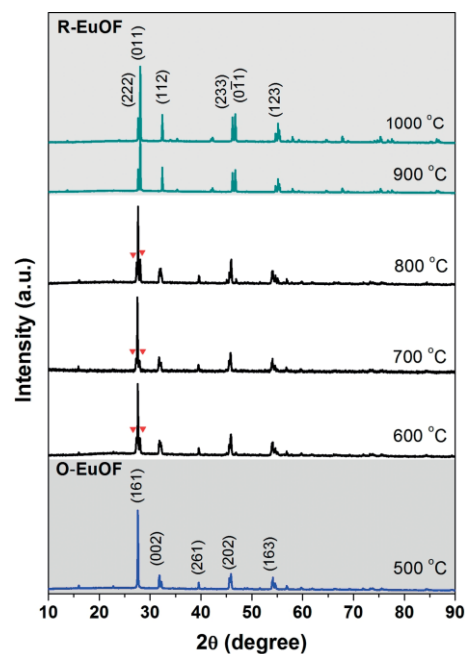


Figure 1. PXRD patterns of the as-synthesized powder samples prepared at different sintering temperatures in the range of 500–1000 °C. The main diffraction peaks of O- and R-EuOF are indexed. Red triangles indicate the diffraction peaks of M-EuOF.

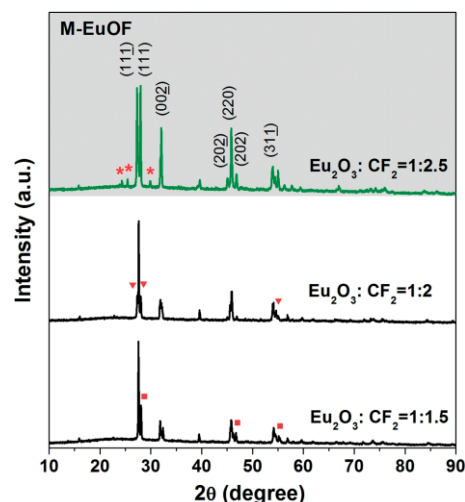


Figure 2. PXRD patterns of the as-synthesized powder samples prepared with different mol ratios of Eu₂O₃/CF₂ = 1:1.5, 1:2 and 1:2.5. The main diffraction peaks of M-EuOF are indexed. Triangles and squares indicate the diffraction peaks of M- and R-EuOF, respectively, and stars indicate the diffraction peaks of EuF₃.

which reveals clear distinctions between the three phases and testifies that M-EuOF is definitely an independent phase instead of a mixed phase of O- and R-EuOF.

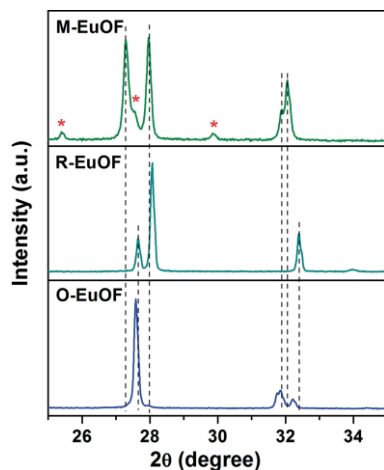


Figure 3. PXRD patterns of O-, M- and R-EuOF in the range of 25–35°. The stars indicate the diffraction peaks of EuF_3 .

On the basis of extensive synthetic experiments and the product phase analyses, a guide to the distribution O-, R- and M-EuOF prepared under specific synthetic conditions, including sintering temperature and F/Eu mol ratio, can be summarized as follows: O- and M-EuOF were obtained at relative low temperatures, generally lower than 800 °C, with M-EuOF being preferred over O-EuOF at a higher F/Eu mol ratio. Pure R-EuOF was observed at higher temperatures and was preferred at a lower F/Eu mol ratio. In addition, it cannot be neglected that R-EuOF coexists with O- and M-EuOF when the temperature and F/Eu ratio are both relatively low, but phase-pure R-EuOF has not been observed under these conditions. DSC measurements on R-EuOF proved a reversible phase transition to O-EuOF at around 461 °C (as shown in Figure S4 in the Supporting Information). A phase-pure product distribution pattern is pictured schematically in Figure S3.

Crystal Structures of O-, M- and R-EuOF

R-EuOF (ICSD #22044) is the only phase known of the three as-obtained europium oxyfluorides. O-EuOF adopts a Vernier-type structure with general formula $\text{RE}_n\text{O}_{n-1}\text{F}_{n+2}$, which is common in lanthanide oxyfluorides with small lanthanides (Y, Lu, Yb, Er).^[12] On the basis of previous experiences in the structure analysis of Vernier-type lanthanide oxyfluorides, O-EuOF was roughly assigned the formula $\text{Eu}_6\text{O}_5\text{F}_8$ ($n = 6$), which was supported by the results of cell parameter refinements. LeBail fitting of the PXRD pattern of O-EuOF using orthorhombic space group *Pcmb* gave cell parameters $a = 5.5649(2)$, $b = 6 \times 5.6441(1)$ and $c = 5.6236(2)$ Å. LeBail fitting of the PXRD pattern for the unknown phase M-EuOF yielded a good result with space group *P121/c1*, $a = 5.5918(9)$, $b = 5.6179(6)$, $c = 5.5907(0)$ Å, $\alpha = \gamma = 90^\circ$ and $\beta = 92.042(2)^\circ$. Rietveld refinement of the PXRD pattern of O-EuOF was performed by using $\text{Y}_6\text{O}_5\text{F}_8$ (ICSD #68949)^[13] as the initial structure model. For brevity, the O/F distribution and disorder were treated by using those in

$\text{Y}_6\text{O}_5\text{F}_8$. Rietveld refinement of M-EuOF was also performed by using the known structure of monoclinic YbOF (ICSD #75557)^[14] as the initial model. The refinement plots for O- and M-EuOF are shown in Figure 4. Detailed atomic positions and other structural parameters for O- and M-EuOF are listed in Tables S1 and S2, respectively, in the Supporting Information.

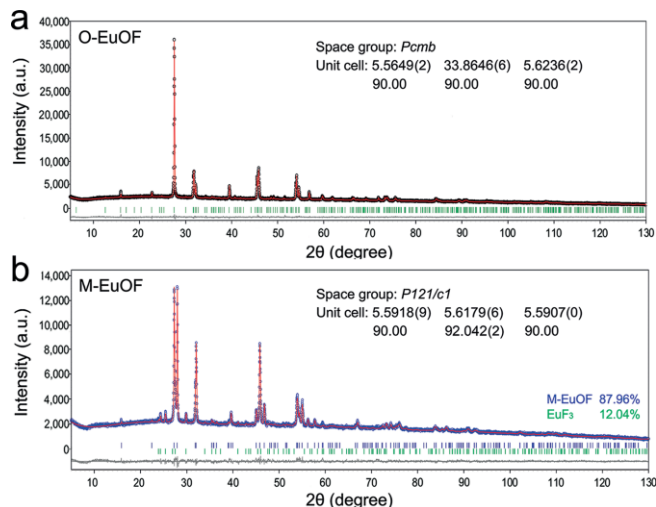


Figure 4. Rietveld refinements of (a) O-EuOF and (b) M-EuOF based on PXRD data.

The crystal structures of O-, M- and R-EuOF are shown in Figure 5. O-EuOF crystallizes in an elongated orthorhombic unit cell derived from the cubic fluorite structure. Partial ordering (8e site) and disorderly distribution of the O/F ligands offer four crystallographic Eu positions with eight-fold coordination and lead to the six-fold elongation of the fluorite structure (i.e., $n =$

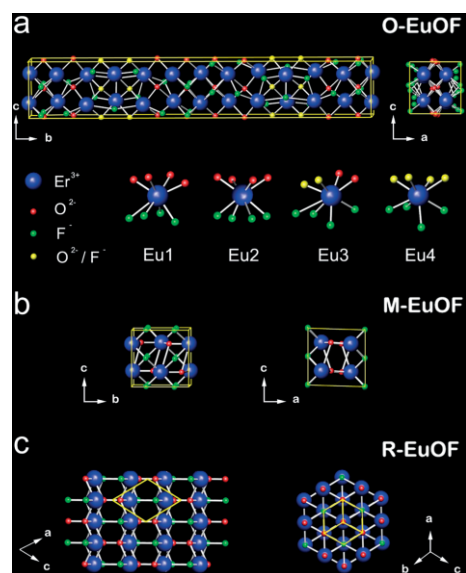


Figure 5. Crystal structures of O-, M- and R-EuOF. (a) Orthorhombic structure of O-EuOF viewed along the a and b axes. The assorted array of O^{2-} and F^- ions offers three different types of Eu^{3+} cation sites. Note that the O^{2-} and F^- anions located at 8e sites shown as green spheres are of disordered distribution. (b) Monolithic structure of M-EuOF viewed along the a and b axes. (c) Rhombohedral structure of R-EuOF presented as (010) and (111) sections.

6, in $a \times nb \times c$). Distinct coordination environments are shown for the four Eu ions despite their normal bond valence sum (BVS) values (around 3+; see Table S1 in the Supporting Information), both in the number of O/F ligands and in their arrangements: Eu1 in C_2^- and Eu2 in C_1^- -symmetric sites with both coordinated to 4 O and 4 F, Eu3 in a C_1^- -symmetric site with 4 F, 2 O and 2 O/F, and Eu4 in a C_s site with 4 O and 4 O/F (Figure 5a). In contrast, the crystal structures of M- and R-EuOF are stoichiometric and highly ordered. The unique Eu site is surrounded by 4 O and 4 F atoms with C_1 and C_{3v} symmetry in M- and R-EuOF, respectively.

Luminescence Properties

As a structural probe, the PL spectra of Eu^{3+} ions are capable to identify the site symmetry in the lattices. The excitation and emission properties of O-, M- and R-EuOF thus offer support for their structural divergence. Figure 6 shows the room-temperature excitation spectra of the as-prepared O-, M- and R-EuOF recorded at their specific emission wavelengths of 610, 609 and 612 nm, respectively, corresponding to the ${}^5\text{D}_0 \rightarrow {}^7\text{F}_2$ transition. The broad bands in the range of 240–310 nm can be assigned to $\text{O}^{2-}(2p) \rightarrow \text{Eu}^{3+}$ charge transfer (CT) excitation, and the series of sharp peaks in the range 300–500 nm can be attributed to 4f–4f transitions of the Eu^{3+} ions. The CT bands of the polymorphs show clear differences. Compared with O- and M-EuOF (CT bands at around 269 nm), there is a slight redshift of the CT band of R-EuOF with the peak at 275 nm. This can presumably be attributed to the nephelauxetic effect caused by the longer Eu–O distances in the R-EuOF compared with those of the other two europium oxyfluorides:^[15] the minimum Eu–O distances are 2.31 (R-EuOF), 2.21 (M-EuOF) and 2.24 Å (O-EuOF), as presented in Table S3 in the Supporting Information. The low-temperature excitation spectra (Figure 7) measured at 77 K show the typical ${}^7\text{F}_0 \rightarrow {}^5\text{D}_{0-4}$, ${}^5\text{G}_{2-6}$, ${}^5\text{L}_6$ and ${}^7\text{F}_0 \rightarrow {}^5\text{D}_1$ transitions.

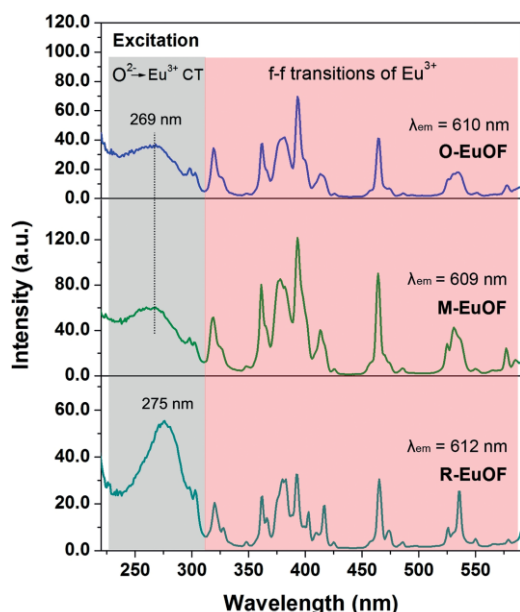


Figure 6. Excitation spectra of O-, M- and R-EuOF at 298 K.

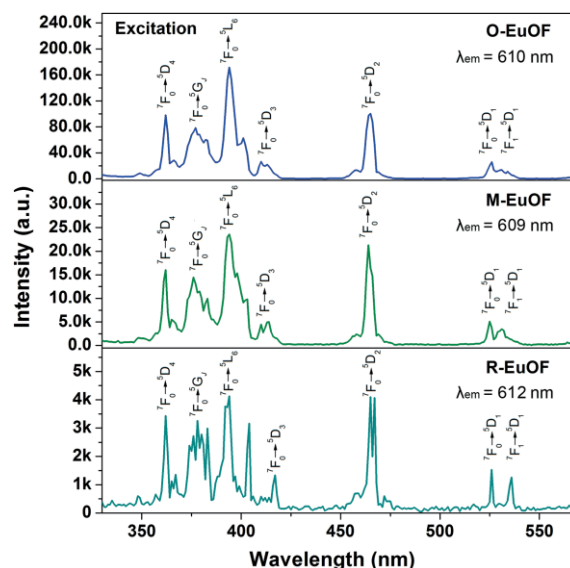


Figure 7. Low-temperature excitation spectra of O-, M- and R-EuOF at 77 K.

The low-temperature (77 K) emission spectra of O-, M- and R-EuOF excited at 394 nm are shown in Figure 8. The typical narrow lines in the spectra can be mainly attributed to Eu^{3+} ${}^5\text{D}_0 \rightarrow {}^7\text{F}_{0-4}$ transitions. Notably, transitions from the higher excited state ${}^5\text{D}_1$ can also be observed in the spectrum of M-EuOF. The electric-dipole transition ${}^5\text{D}_0 \rightarrow {}^7\text{F}_2$ has the highest emission intensity, and the intensity of the magnetic-dipole transition ${}^5\text{D}_0 \rightarrow {}^7\text{F}_1$ is quite low in all the spectra, which means that Eu^{3+} ions occupy the sites without inversion symmetry. The presence of the ${}^5\text{D}_0 \rightarrow {}^7\text{F}_0$ transition reveals that Eu^{3+} sites exist in all three europium oxyfluorides with C_s , C_n or C_{nv} symmetry, which is consistent with the results of structure refinement (see Figure S5 in the Supporting Information). Because the EuF_3 impurity in M-EuOF may significantly influence the intensity of ${}^5\text{D}_0 \rightarrow {}^7\text{F}_1$ (Figure S6), we have not used the ${}^5\text{D}_0 \rightarrow {}^7\text{F}_2 / {}^5\text{D}_0 \rightarrow {}^7\text{F}_1$

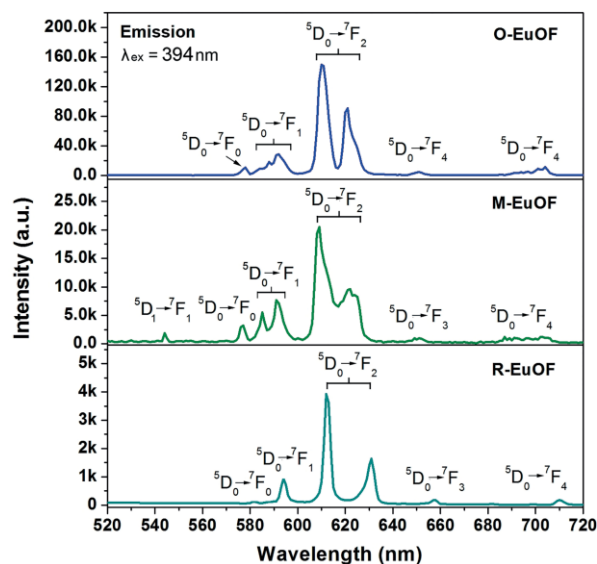


Figure 8. Low-temperature emission spectra of O-, M- and R-EuOF at 77 K.

ratio to determine the average symmetry of the lanthanide ions.

There are also some discrepancies in the low-temperature emission spectra of O-, M- and R-EuOF. First, the splitting of the $^5D_0 \rightarrow ^7F_2$ transition is larger in R-EuOF than in the other polymorphs, which has been found in other rhombohedral REOF, for example, LaOF and YOF.^[16] By comparison, the $^5D_0 \rightarrow ^7F_2$ transitions for M- and O-EuOF show broadening or multiple splitting, which can be attributed to an Eu^{3+} site with lower symmetry (C_1 in M-EuOF) and the presence of multiple Eu^{3+} sites (C_1 , C_2 and C_s in O-EuOF). Also, the high-level transition $^5D_1 \rightarrow ^7F_1$ is only observed in the spectrum of M-EuOF, which is supposedly related to its larger Eu–Eu distance. Transitions from higher levels $^5D_{1-3}$ are generally sensitive to Eu^{3+} doping concentration for the cross-relaxation process, and these transitions are quenched in the spectra of O- and R-EuOF. It is also known that cross-relaxation is an energy-transfer process between two identical active ions with matching energy gaps.^[17] The energy transfer is considered to be dominated by electric exchange interactions rather than multipolar transfer interactions when the distances between active ions are less than 5 Å.^[18] In our cases, the minimum distances between neighbouring Eu^{3+} ions are 3.64 (O-EuOF), 3.68 (R-EuOF) and 3.85 Å (M-EuOF; all neighbouring Eu–Eu distances below 4 Å are listed in Table S4 in the Supporting Information). Hence, the probability (P_{ET}) of adjacent Eu–Eu energy transfer can be determined from $P_{\text{ET}} = C \exp(-2R/L)$, in which R is the distance between the energy donor–acceptor pair, C is the Eu–Eu interaction constant, and L is the effective Bohr radius. Accordingly, the longer ionic distances in M-EuOF lower the probability of energy transfer between two Eu neighbours, and thus it exhibits a weaker cross-relaxation process, which preserves the higher-level transition $^5D_1 \rightarrow ^7F_1$ in the emission profile.

Luminescence Decays

The luminescence decays of O-, M- and R-EuOF were measured at room temperature at 610, 609 and 612 nm, respectively, which correspond to their $^5D_0 \rightarrow ^7F_2$ transition bands. The emission decay profiles are shown in Figure 9, which fit the follow-

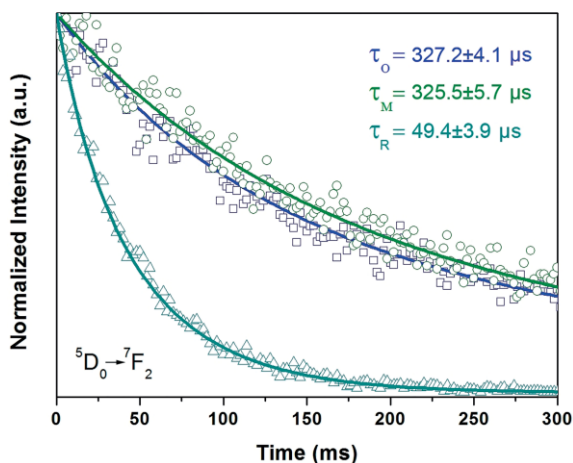


Figure 9. Decay curves of O-, M- and R-EuOF measured at 610, 609 and 612 nm, respectively ($^5D_0 \rightarrow ^7F_2$).

ing biexponential Equation (1), and the average lifetime τ_x ($x = \text{O, M, R}$ for O-, M- and R-EuOF) is defined by Equation (2):^[19]

$$I = I_0 + A_1 \exp(-t/\tau_1) + A_2 \exp(-t/\tau_2) \quad (1)$$

$$\tau_x = (A_1 \tau_1^2 + A_2 \tau_2^2) / (A_1 \tau_1 + A_2 \tau_2) \quad (2)$$

in which I_0 is the initial luminescence intensity at time $t = 0$, A_1 and A_2 are the intensities of two components, and τ_1 and τ_2 are the decay times of the two components. The fitting parameters are provided in Table S5 in the Supporting Information. The observation of a second component is reasonable in Eu^{3+} -heavily-doped samples, due to the increased possibility of Eu^{3+} ions occupying surface sites.

Information on the PL mechanism can be obtained from the analysis of the decay curves, as follows. First, the excitation process in the decay curve was not found in all three samples. This phenomenon suggests that the energy-migration process between Eu^{3+} ions is too fast to be observed due to the ultra-short distances between Eu^{3+} ions caused by their high concentration in the lattices.^[20] Compared with lanthanide oxyfluorides with low Eu^{3+} doping levels showing lifetimes in the millisecond region, all the present samples exhibit much shorter lifetimes in the range of 49–327 μs due to the serious cross-relaxation between neighbouring Eu^{3+} ions. In addition, the high Eu^{3+} concentration is also responsible for the biexponential behaviour of the decay curves, because the Eu^{3+} ions on the surface can be considered within an emerging coordination environment.

Conclusions

We have reported herein the controllable synthesis of orthorhombic, monoclinic and rhombohedral europium oxyfluorides by a facile PTFE fluorination route. Phase selectivity was achieved by simply controlling the F/Eu mol ratio and the reaction temperature. O-, M- and R-EuOF show distinct excitation and emission profiles in the room- and low-temperature PL spectra that are associated with specific Eu^{3+} site symmetries in the three lattices. An exceptional high-level transition ($^5D_1 \rightarrow ^7F_1$) is observed in M-EuOF, which will always disappear in materials with a high concentration of dopant due to cross-relaxation. The larger Eu–Eu distances in M-EuOF, which can weaken the cross-relaxation effect between neighbouring Eu^{3+} ions, are considered responsible for this phenomenon. These results demonstrate that lanthanide oxyfluoride with various polymorphisms is a perfect platform for comparative investigations of structure-dependent PL properties and may find applications as PL or UC PL host materials.

Experimental Section

Material Syntheses: Powder samples of O-, M- and R-EuOF were synthesized by a fluorination route using europium oxide as the raw material and PTFE as the fluorinating agent.^[21] In a typical procedure, Eu_2O_3 (0.352 g, 1 mmol; >99.5%) and PTFE powder (CF_2 , 0.75–0.125 g, 1.5–2.5 mmol; >99%) were weighed and thoroughly ground with ethanol for several minutes. The resulting fine powder

was sealed in an alumina crucible and slowly heated to the target temperature (400–1000 °C) at a heating rate of 5 °C/min. After holding at the reaction temperature for 5 h, the furnace was cooled to room temperature with the power switched off.

Characterization: PXRD data of all the samples were collected at room temperature (25 °C) with a Bruker D8 Advance diffractometer (Cu-K_α) using a germanium monochromator. Data in the 2θ range of 5–130° were collected in steps of 0.02° at 1 s per step under tube conditions of 40 kV and 40 mV. Least-squares refinement of the cell parameters and atomic positions of the samples were performed by using the known structures of YOF and YbOF stored in the ICSD database as the initial models.^[22] Room-temperature PL spectra were recorded with an Hitachi F-4600 spectrophotometer and low-temperature PL spectra (77 K) were measured with a stable and transient spectrophotometer (JY HORIBA FluoroLog-3). Room-temperature PL decay curves were collected by using an FLS980 spectrophotometer equipped with a 150 W Xe lamp as the excitation source.

Acknowledgments

This work was supported by the National Natural Science Foundation of China (51602119), the Natural Science Foundation of Education Department of Henan (17A150014), and the Key Project of Science and Technology of Zhengzhou (153PKJGG139).

Keywords: Structure elucidation · Oxyfluorides · Europium · Luminescence · Polymorphism

- [1] a) X. Sun, Y. W. Zhang, Y. Du, Z. G. Yan, R. Si, L. You, C. Yan, *Chem. Eur. J.* **2007**, *13*, 2320–2332; b) T. Grzyb, S. Lis, *Inorg. Chem.* **2011**, *50*, 8112–8120; c) L. Armelao, G. Bottaro, L. Bovo, C. Maccato, M. Pascolini, C. Sada, E. Soini, E. Tondello, *J. Phys. Chem. C* **2009**, *113*, 14429–14434; d) Y. Du, Y. Zhang, L. Sun, C. Yan, *J. Phys. Chem. C* **2008**, *112*, 405–415; e) M. Shang, G. Li, X. Kang, D. Yang, D. Geng, C. Peng, Z. Cheng, H. Lian, J. Lin, *Dalton Trans.* **2012**, *41*, 5571–5580; f) Y. Du, Y. Zhang, Z. Yan, L. Sun, C. Yan, *J. Am. Chem. Soc.* **2009**, *131*, 16364–16365; g) M. Shang, D. Geng, X. Kang, D. Yang, Y. Zhang, J. Lin, *Inorg. Chem.* **2012**, *51*, 11106–11116; h) Y. Zhang, X. Li, X. Kang, Z. Hou, J. Lin, *Phys. Chem. Chem. Phys.* **2014**, *16*, 10779–10787; i) K. Zheng, Y. Liu, Z. Liu, Z. Chen, W. Qin, *Dalton Trans.* **2013**, *42*, 5159–5166; j) T. Grzyb, A. Tyminski, *J. Alloys Compd.* **2016**, *660*, 235.
- [2] T. Passuello, F. Piccinelli, M. Trevisani, M. Giarola, G. Mariotto, L. Marciniak, D. Hreniak, M. Guzik, M. Fasoli, A. Vedda, V. Jary, M. Nikl, V. Causin, M. Bettinella, A. Speghini, *J. Mater. Chem.* **2012**, *22*, 10639–10649.
- [3] B. Hyde, A. Bagshaw, S. Anderson, M. O’Keeffe, *Annu. Rev. Mater. Sci.* **1974**, *4*, 43–92.
- [4] a) O. Janka, T. Schleid, *Eur. J. Inorg. Chem.* **2009**, 357–360; b) N. Rakov, R. B. Guimaraes, W. B. Lozano, G. S. Maciel, *J. Appl. Phys.* **2013**, *114*, 043517(1–7).
- [5] See ref.^[1b]
- [6] a) R. Jagannathan, M. Kottaisamy, *J. Phys. Condens. Matter* **1995**, *7*, 8453–8467; b) M. Zhao, Z. Xia, M. S. Molokeev, L. Ning, Q. Liu, *Chem. Mater.* **2017**, *29*, 6552–6559; c) M. Chen, Z. Xia, M. S. Molokeev, T. Wang, Q. Liu, *Chem. Mater.* **2017**, *29*, 1430–1438.
- [7] a) D. Ananias, F. A. A. Paz, D. S. Yufit, L. D. Carlos, J. Rocha, *J. Am. Chem. Soc.* **2015**, *137*, 3051; b) W. J. Kim, B. Min, D. Pradhanc, Y. Sohn, *CrystEngComm* **2015**, *17*, 1189–1200; c) Y. Li, J. Zhang, X. Zhang, Y. Luo, S. Lu, X. Ren, X. Wang, L. Sun, C. Yan, *Chem. Mater.* **2009**, *21*, 468–475; d) X. Zhang, M. Wang, J. Ding, J. Deng, C. Ran, Z. Yang, *Dalton Trans.* **2014**, *43*, 5453–5461.
- [8] D. Tu, Y. Liu, H. Zhu, R. Li, L. Liu, X. Chen, *Angew. Chem. Int. Ed.* **2013**, *52*, 1128–1133; *Angew. Chem.* **2013**, *125*, 1166.
- [9] See ref.^[4b]
- [10] a) Y. Wang, T. Wen, H. Zhang, J. Sun, M. Zhang, Y. Guo, W. Luo, M. Xia, Y. Wang, B. Yang, *J. Phys. Chem. C* **2014**, *118*, 10314–10320; b) T. Wen, Y. Zhou, Y. Guo, C. Zhao, B. Yang, Y. Wang, *J. Mater. Chem. C* **2016**, *4*, 684–690.
- [11] T. Wen, R. Ding, Y. Zhou, Y. Si, B. Yang, and Y. Wang, *Eur. J. Inorg. Chem.*, 10.1002/ejic.201700658.
- [12] a) T. Wen, W. Luo, Y. Wang, M. Zhang, Y. Guo, J. Yuan, J. Ju, F. Liao, B. Yang, *J. Mater. Chem. C* **2013**, *1*, 1995–2001; b) W. Luo, Y. Wang, Y. Chen, T. Wen, M. Liu, Y. Wang, F. Liao, J. Lin, *J. Mater. Chem. C* **2013**, *1*, 5711–5717.
- [13] D. M. Bevan, J. Mohyla, B. Hoskins, R. Steen, *Eur. J. Solid State Inorg. Chem.* **1990**, *27*, 451–465.
- [14] A. Taoudi, J. P. Laval, B. Frit, *Mater. Res. Bull.* **1994**, *29*, 1137–1147.
- [15] T. Grzyb, M. Węclawiak, T. Pędziński, S. Lis, *Opt. Mater.* **2013**, *35*, 2226–2233.
- [16] a) See ref.^[4b]; b) see ref.^[1b]
- [17] E. Okamoto, M. Sekita, H. Masui, *Phys. Rev. B* **1975**, *11*, 5103–5111.
- [18] a) J. Wang, R. Deng, M. MacDonald, B. Chen, J. Yuan, F. Wang, D. Chi, T. A. Hor, P. Zhang, G. Liu, Y. Han, X. Liu, *Nat. Mater.* **2014**, *13*, 157–162; b) M. Inokuti, F. Hirayama, *J. Chem. Phys.* **1965**, *43*, 1978.
- [19] T. Fujii, K. Kodaira, S. Kawauchi, N. Tanaka, H. Yamashita, M. Anpo, *J. Phys. Chem. B* **1997**, *101*, 10631–10637.
- [20] See ref.^[1b]
- [21] S. Dutton, D. Hirai, R. Cava, *Mater. Res. Bull.* **2012**, *47*, 714–718.
- [22] a) D. M. Bevan, J. Mohyla, B. Hoskins, R. Steen, *Eur. J. Solid State Inorg. Chem.* **1990**, *27*, 451–465; b) see ref.^[14]

Received: July 25, 2017